Short-Circuit Fault Models Analysis for a Planetary Rover DC Motor Actuator Using a Kalman Filter Model-Based Fault Detection Approach

Salim Al Oufi*, Euan McGookin†, and Kevin Worrall‡
School of Engineering, University of Glasgow, Glasgow, G12 8QQ UK e-mails: * s.al-oufi.1@research.gla.ac.uk;
† Euan.mcgookin@glasgow.ac.uk;
‡ kevin.worrall@glasgow.ac.uk.

***Abstract*—The actuators of the Planetary Exploration Rover (PER) can fail, or its performance is decreased by hidden faults, for example, a short-circuit (SC). Therefore, detecting and isolating faults is essential to increase the PER reliability. Since investigating such faults using a physical system is extremely expensive and time-consuming, an accurate PER mathematical model (or digital twin) with DC motor's SC fault representation can form the basis of a simulation tool for investigating this type of fault. Two particular SC fault models are investigated in this work. This involves investigating the effects of these faults on the performance of the PER and the health monitoring process. This study proposes a Kalman Filter (KF) technique as a model-based fault detection method to investigate the SC fault models' accuracy and detection.**

I. Introduction

The exploration of planetary surfaces by Planetary Exploration Rovers (PER) has become an essential aspect of space missions, providing valuable scientific data and insights into the geology and potential habitability of other celestial bodies [1]. Future PERs need to be highly autonomous or semi-autonomous, as they must perform tasks with minimal human input. This necessitates a robust system that can detect, isolate, and recover from faults, ensuring the rover's continued operation and mission success. The space environment poses numerous challenges for PER health, including extreme temperatures, radiation, and dust, which can lead to component degradation and failure. Implementing an effective health monitoring system can mitigate these risks and extend the rover's operational life.

The design of a health monitoring system can be achieved through simulation, which involves the development of fault models that accurately represent the behaviour of the rover's subsystems under various fault conditions [2]. One of the critical systems in a planetary rover is the actuators, which are responsible for the rover's mobility and manipulation capabilities. Failure of the actuators system can have severe consequences for the mission, rendering the rover immobile or unable to perform its tasks.

The PER's DC motor actuators can experience various faults [3]. DC motor failure or a reduction in its efficiency can be induced by many reasons [4]. Sticking motor, which is a phase where the torque and speed from the DC motor are reduced, and short-circuit are common DC motor faults. Contamination or misalignment in the DC motor would develop a frictional force applied on the motor's shaft, causing a sticking fault [3]. Low winding insulation due to conditions such as overheating, corrosion, or physical damage causes a SC fault. The consequences of the SC fault on the motor could be minor as a slight reduction in the motor efficiency going up to overheat, and overload escalated to a complete failure [3]. Therefore, detecting the SC fault in its early stage is desirable to avoid total motor failure.

Fault detection processes are classified into two general classes that are data-based and model-based methods[5]. The data-based method analyses knew previous large data sets of the system measurement to detect the faults, whereas the model-based approach compares the system behaviour with a model description of the system to detect the fault [2]. The model-based method is preferred for the flexibility of giving a wider range of operational possibilities, whereas the data-based method is tied by complex different data sets. Various studies have been done on fault detection and isolation methods for electrical motors' winding short-circuit faults. [6] review some studies in fault diagnosis techniques of inter-turn short circuit fault and irreversible demagnetisation fault. A statistical Hidden Markov-based model was developed by [7] to detect a simulated inter-turn short circuit fault on a DC motor model. A KF-based fault detection method was investigated by [8] for online short circuit fault detection on a physical synchronous motor.

This paper investigates two models of short-circuit faults in a rover's DC motor actuator, analyzing the rover's behaviour under these fault conditions and utilizing a KF model-based fault detection approach to identify and isolate the faults. The KF is a well-established technique for estimating the state of a dynamic system, making it an ideal candidate for model-based fault detection in rover actuators' health monitoring. This paper investigates the detectability and classification of two SC fault models using a KF model-based fault detection method and analyses the behaviour of the PER with respect to the fault models and the fault detection and isolation process.

The primary aim of this paper is to compare the two short-circuit fault models for the rover's DC motor actuator and investigate the performance of a model-based KF algorithm for fault detection. By analyzing the rover's behaviour under these fault conditions and evaluating the effectiveness of the KF in detecting and isolating the faults, this research contributes to the development of more reliable and resilient health monitoring systems for planetary rovers, ultimately increasing their operational lifespan and mission duration.

II. Four Wheel PER model

In this study, rigid-body dynamics and kinematics are implemented in a mathematical model (or digital twin) of a 4-wheel rover from

Lynxmotion [9]. The model's kinematics are defined by references to the Earth-fixed frame and the rover's body-fixed frame (Fig.1).

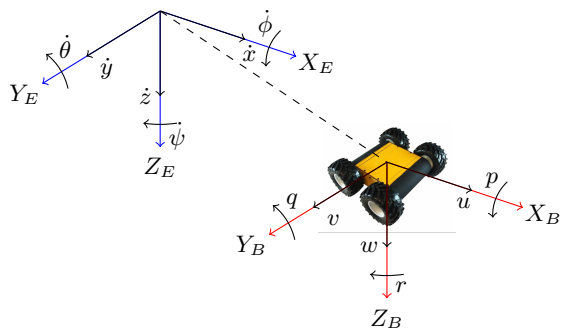

Fig. 1. Earth-fixed (X_E, Y_E, Z_E (blue)) and rover body-fixed axes (X_B, Y_B, Z_B (red))for the modelled four wheel Lynxmotion rover. Credit: [9]

The matrix representation in Equation (1) [10] describes the rover's equation of motion.

$$\begin{aligned} \boldsymbol{M}\dot{\boldsymbol{\nu}} + \boldsymbol{C}(\boldsymbol{\nu})\boldsymbol{\nu} &= \boldsymbol{\tau} - \boldsymbol{D}(\boldsymbol{\nu}) - \boldsymbol{g}(\boldsymbol{\eta}) \\ \dot{\boldsymbol{\eta}} &= \boldsymbol{J}(\eta)\boldsymbol{\nu} \end{aligned} \tag{1}$$

Here $\boldsymbol{M}$ is the mass and inertia matrix, $\boldsymbol{\nu} = [u, v, w, p, q, r]$ is the body-fixed velocity vector, $\boldsymbol{C}(\boldsymbol{\nu})$ is the Coriolis matrix, $\boldsymbol{D}(\boldsymbol{\nu})$ is the damping matrix, $\boldsymbol{g}(\boldsymbol{\eta})$ represents the gravitational forces and moments, $\boldsymbol{\eta} = [x, y, z, \phi, \theta, \psi]$ is the inertially fixed position/orientation vector, $\boldsymbol{J}(\boldsymbol{\eta})$ is an Euler matrix representing the trigonometric transformation from the body-fixed reference frame to the earth fixed reference frame, and the $\boldsymbol{\tau}$ represents the reactive forces and moments matrix.

The Lynxmotion DC motor specified parameters' values are shown in Table I.

TABLE I
SPECIFICATIONS OF THE DC MOTOR [11]

Specifications
R: 4Ω
L: 0.1m.H
K_t: 0.35N.m/A
K_e: 0.35V.s/rad
b: 0.008N.m
J: 0.005Kg.m^2
τ_L: 0.05N.m

The actuators and the rigid body's equation of motion are the two main subsystems that operate the rover. The rigid body equation of motion is described in Equation 1, whereas the actuators are modelled as DC motors. The equations of a DC motor describing the electrical and mechanical system are represented in Equations (2) and (3) [4].

$$V(t) = L\dot{I}(t) + RI(t) + K_e\omega(t) \tag{2}$$

$$J\dot{\omega}(t) = K_t I(t) - b\omega(t) - \tau_L(t) \tag{3}$$

In this equations, V is the input in voltages I is the armature current, L the armature inductance, R the coil resistance, ω the rotational velocity of the motors, J is the moment of inertia for the rotor, b is viscous friction coefficient, τ_L is the load torque, and Ψ the flux linkage, which is defined as K_e (emf constant) and K_t (torque constant). The surge velocity and heading are controlled by two PID controllers, which are implemented to produce signals for the desired voltage inputs that are provided to the DC motors. Line-of-sight (LoS) algorithm is implemented for the guidance and navigation system of the rover. Fig. 2 shows the control, guidance and navigation system for the rover, where ψ and ψ_d are the measured and desired heading, respectively. The rover's measured position is denoted by x and y, and its measured and desired velocities are $\vec{v}$ and $\vec{v}_d$, respectively.

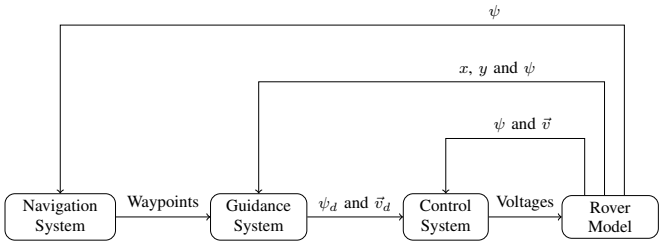

Fig. 2. PER guidance, navigation and control system. Credit: [9]

III. SHORT-CIRCUIT IMPLEMENTATION

The SC fault occurs in the armature winding of a DC motor when the winding has low insulation, which increases the current in the armature winding, as illustrated in Fig 3. Excessive heat is generated by the increased current that decreases the capability of the DC motor. Detecting and isolating this fault in the early stage would reduce the total damage to the DC motor by following an appropriate recovery action.

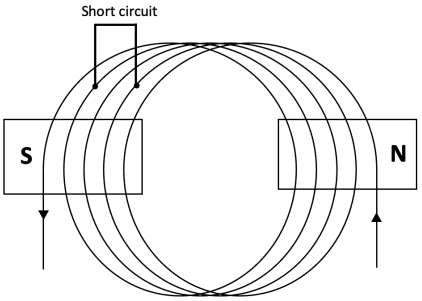

Fig. 3. Armature winding with short-circuit fault

In this study, two models of the SC fault are implemented as a reduction ratio δ, which is the percentage of the short-circuited winding. In the first model (Model A), the SC fault ratio δ is applied to the armature winding resistance and inductance as proposed by [7]. The effect of the SC fault on the flux-linkage is neglected in Model A. In the second model (Model B), the SC fault ratio δ is applied to the armature coil's resistance, inductance and flux-linkage as proposed by [12]. Calculating the effect of the fault on the flux-linkage could be crucial for accurate fault modelling.

The following equations calculate the resistance (R), inductance (L) and flux-linkage (Ψ) of the healthy part of a short-circuited armature coil.

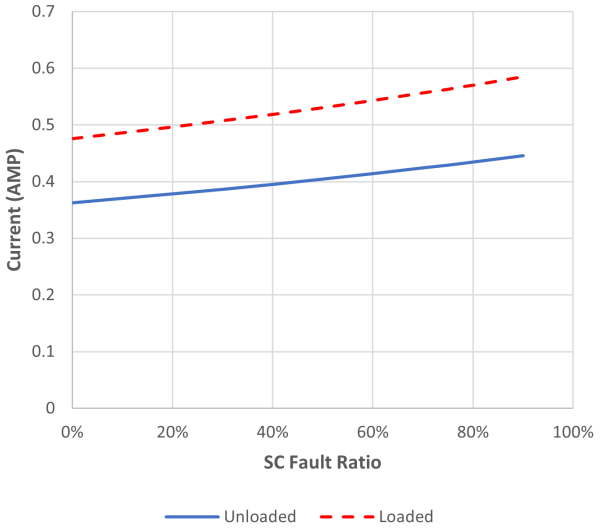

Fig. 4. Current behaviour for L & UL motor with SC fault from 0% to 90% ratio for SC fault Model A

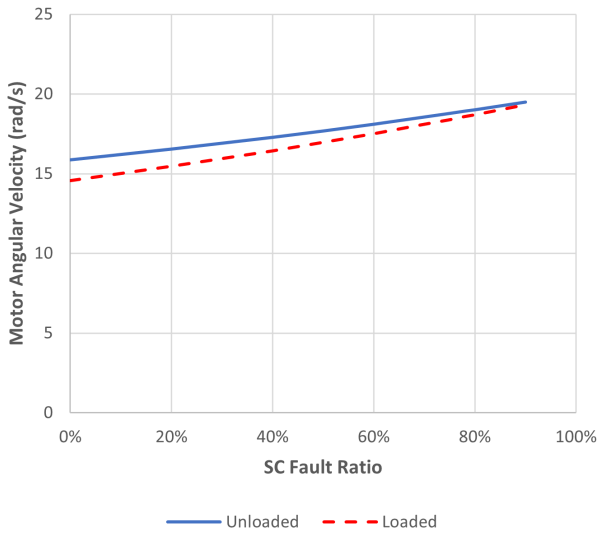

Fig. 5. Angular velocity behaviour for L & UL motor with SC fault from 0% to 90% ratio for SC fault Model A

$$R_1 = \rho\frac{l(1-\delta)}{A} = R(1-\delta) \tag{4}$$

$$L_1 = \mu\frac{N^2(1-\delta)^2 A}{l(1-\delta)} = L(1-\delta) \tag{5}$$

$$\Psi_1 = 2BNlr_a(1-\delta)^2 = \Psi(1-\delta)^2 \tag{6}$$

In these equations, R_1, L_1 and Ψ_1 are the armature resistance (Ω), inductance (H) and flux-linkage (K_e ($V.s/rad$), K_t ($N.m/A$)) respectively. ρ is the resistivity (Ωm), A is the cross-sectional area of the coil(m^2), l is the length of the conductor (m), μ is the vacuum permeability constant (H/m), N is the number of turns in the armature, B is the strength of the magnetic field ($Tesla$), and r_a is the radius of the motor armature (m).

A. Results

The Lynxmotion rover's 12 $Volts$ DC motor model specified in Section II is implemented in simulation with fixed voltage input 7 $Volts$. The fault is introduced to the DC motor with several ratios (percentages) starting with the healthy motor case 0% to 90% SC fault with an increment of 10%, note that 100% SC fault means the motor would fail to operate; where the loaded (L) and unloaded (UL) motor cases are examined. The current behaviour of the DC motor is investigated with several SC fault Model A ratios as in Fig. 4.

The current is increasing linearly, raising the SC fault ratio from 0.36-0.46 Amps for the unloaded motor and 0.47-0.58 Amps for the loaded motor. The coil current's reaction to the SC fault is minor, and the 90% fault ratio increased by about 0.1 amps compared to the healthy motor. Fig. 5 shows the angular velocity behaviour of the DC motor with SC fault Model A.

Motor speed is increased linearly as the SC ratio increases from 15.9-19.9 rad/s for the unloaded motor and 14.6-19.9 rad/s for the loaded motor. The speed is reduced with the added load and increased with drift when increasing the fault ratio, that the motor's speed for both loaded and unloaded are similar for 90% fault ratio.

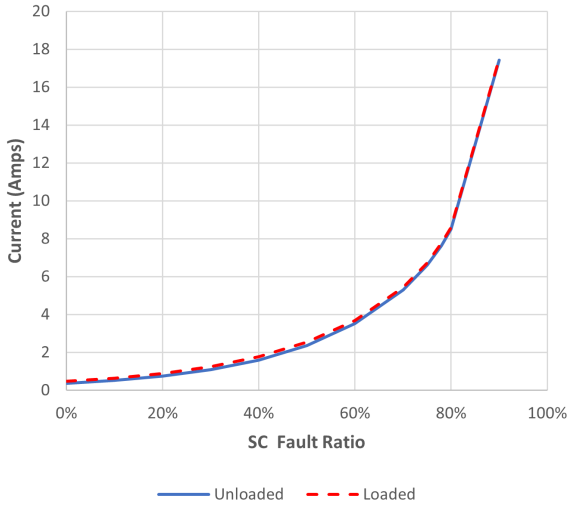

Fig. 6. Current behaviour for L & UL motor with SC fault from 0% to 90% ratio for SC fault Model B

Fig.6 shows the current behaviour of the DC motor with SC fault Model B ratios ranging from $0\% - 90\%$.

Increasing the SC fault ratio draws current exponentially in the DC motor. The SC fault makes the motor draw current more than the maximum rated current in the specified DC motor datasheet, which is 1.6 amps when the SC fault ratio is above 40%. Considering that the motor would be overloaded and fail if the current goes above the rated current; the 40% SC fault ratio is the maximum when the inputted voltage is 7 Volts because the current exceeded the manufacturer classified maximum current. Fig. 7 shows the angular velocity behaviour of the DC motor with SC fault Model B.

The velocity increases with rising the fault percentage until 50% fault ratio, then the velocity decreases. The reason for the increase in speed is the increase in the current. Then the effect of the fault ratio

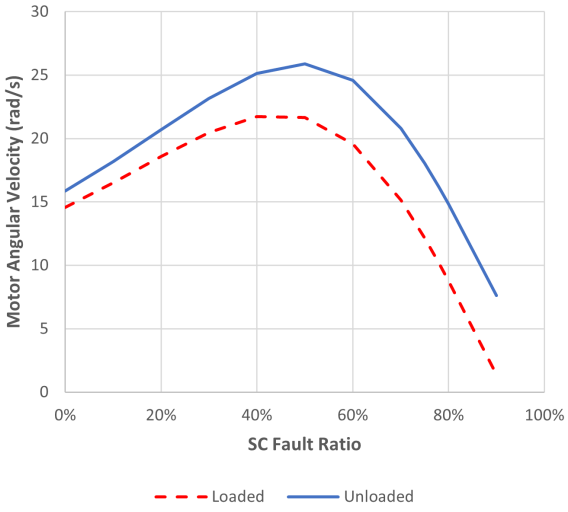

Fig. 7. Angular velocity behaviour for L & UL motor with SC fault from 0% to 90% ratio for SC fault Model B

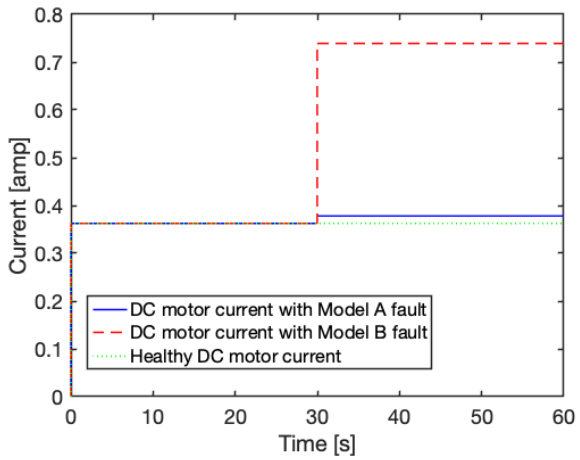

Fig. 8. Current Response Comparison of Faultless and Faulty DC Motor for both SC fault models (A and B)

on the flux-linkage (K_e, K_t) reduction became more dominant than the impact of the high current, causing a decrease in the speed. The velocity is decreased with drift when the fixed load is added with the increase of the SC fault ratio. The impact of the load will reduce the speed that the reduction would drift down when the SC fault ratio is increased compared with the unloaded DC motor.

Fig. 8 and 9 show respectively the current and angular velocity behaviour of both faulty DC motor Models (A and B) 40% fault ratio compared to healthy responses. Although the DC motor current and angular velocity are increased in both SC fault models, it is noticeable that the fault Model B has a much greater influence on the DC motor responses than Model A.

IV. Kalman Filter Fault Detection and Isolation (FDI)

KF is an iterative state estimation observer utilized in a linear dynamic system with noisy measurements taken over time to anticipate

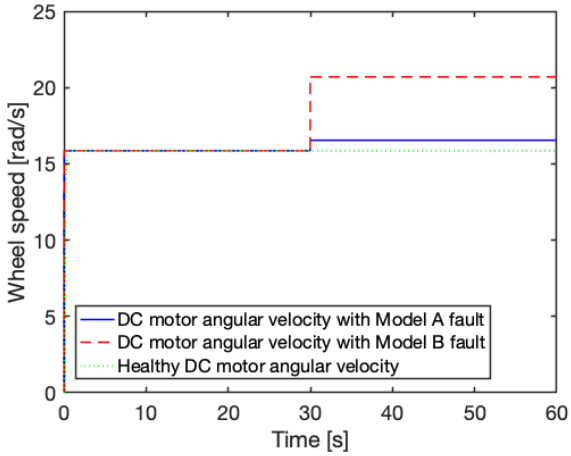

Fig. 9. Angular Velocity Response Comparison of Faultless and Faulty DC Motor for both SC fault models (A and B)

the state of the dynamic system [13].

In this study, SC Fault detection can be achieved by supervising the faulty model measurements of the PER's states. Residuals are generated by analysing these measurements using a model-based KF. A threshold would then be selected for the residuals to detect the occurrence of a fault. A model-based KF fault detection method is used to develop residuals for each SC fault Model (A and B). The generated residuals are analysed to investigate the detectability of both SC fault models. The equation format of the KF can be written as first the prediction step:

$$\hat{x}(k+1 \mid k) = \boldsymbol{A}\hat{x}(k \mid k) + \boldsymbol{B}u(k) \tag{7}$$

$$\hat{y}(k) = \boldsymbol{C}\hat{x}(k+1 \mid k) \tag{8}$$

$$P(k+1 \mid k) = \boldsymbol{A} \cdot P(k \mid k) \cdot \boldsymbol{A}^T + Q(k) \tag{9}$$

$\hat{x}(k+1 \mid k)$ is the predicted state, $\hat{x}(k \mid k)$ is the previous state, $\boldsymbol{A}$ is state transition matrix, $\boldsymbol{B}$ is control matrix, $u(k)$ is input, $\hat{y}(k)$ is the estimated output, $\boldsymbol{C}$ is observation matrix, $P(k+1 \mid k)$ is the predicted error covariance, $P(k \mid k)$ is the previous error covariance, and $Q(k)$ is the state noise.

The FDI, when using the KF estimator, is based on the residual (innovation) $r(k)$ Equation (10) calculated from the sensor measurement or the measured states of the rover's DC motor $y(k)$ and the KF estimated output state $\hat{y}(k)$.

$$r(k) = y(k) - \hat{y}(k) \tag{10}$$

The equations of the KF correction step:

$$K(k) = \frac{P(k+1 \mid k) \cdot \boldsymbol{C}^T}{\boldsymbol{C}.P(k+1 \mid k) \cdot \boldsymbol{C}^T - n(k)} \tag{11}$$

$$\hat{x}(k+1 \mid k+1) = \hat{x}(k+1 \mid k) + K(k) \cdot r(k) \tag{12}$$

$$P(k+1 \mid k+1) = (I - K(k).\boldsymbol{C})P(k \mid k) \tag{13}$$

Here $K(k)$ represents the Kalman gain, $n(k)$ is the measurement noise, and I is the identity matrix.

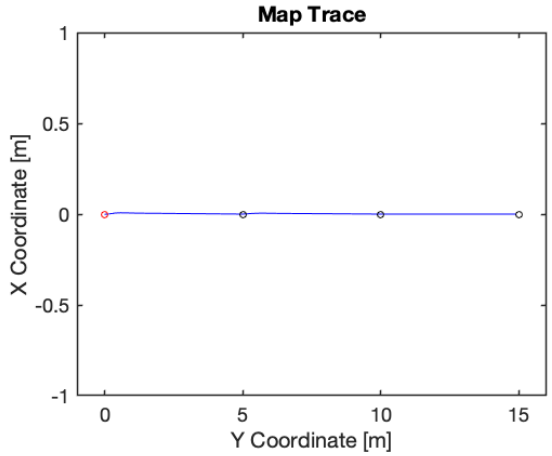

Fig. 10. Straight line path of the rover, where 30% ratio SC fault (Model A) introduced to the first actuator. The starting point is shown as a red circle, each waypoint with black circles, and the rover path is shown in blue

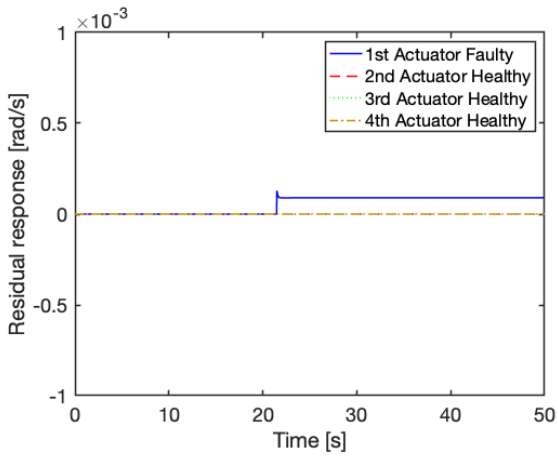

Fig. 11. Residuals of four wheels velocities with 30% SC fault (Model A) ratio

V. Results

Two sets of rover implementations were developed to investigate the two SC fault models (A and B). The rover model is implemented in a 2D closed-loop control system where a couple of waypoints are outfitted on a straight-line path. The SC fault is introduced during the simulation to one actuator of the rover to interrogate the detectability of each SC fault model. Four residuals are derived from the KF model-based FDI considering the angular velocity measurements of each rover's four wheels. The residuals are obtained from Equation (10), where $r_v(k)$ is the residual response to the velocity of the rover's DC motor. A threshold would then be selected for the residuals to detect the occurrence of a fault. To minimise computational complexity, fixed thresholds are picked in this work.

A. Model A

Fig. 10 illustrates the path of the rover as it follows desired waypoints in a straight line in a 2D environment while introducing the SC fault of (Model A) to one actuator of the rover after reaching the first waypoint. It can be seen that the rover follows the path successfully even with one faulty actuator.

Fig. 11 shows the velocities residuals' responses when a 30% SC fault ratio is introduced to one actuator of the rover's four wheels during the simulation.

A small increase in the residual response representing the faulty actuator after the fault was introduced compared to the other residuals representing healthy actuators. If the uncertain dynamics of the DC motor are added to the model, the small threshold could incorrectly detect a SC fault.

B. Model B

Fig. 12 shows the rover's path as it travels in a straight line in a 2D environment while, after arriving at the first waypoint, introducing the SC fault of (Model B) to one actuator of the rover. It can be seen from Fig. 12 that the introduced fault (SC Model B) to one actuator of the rover caused a small deviation from following the straight line path but the closed-loop control made the rover still able to follow the waypoints path.

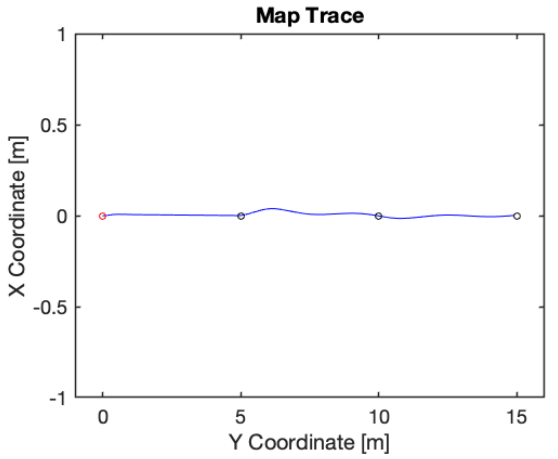

Fig. 12. Straight line path of the rover, where 30% ratio SC fault (Model B) introduced to the first actuator. The starting point is shown as a red circle, each waypoint with black circles, and the rover path is shown in blue

The residuals' responses generated from the four wheels' velocities are shown in Fig. 13. The introduced fault of 30% ratio SC Model B, increased the residual from zero to above $0.008 rad/s$ indicating the possibility of detecting the faulty actuator by setting a threshold with value under $0.008 rad/s$.

Upon thoroughly examining the rover's path-following behaviour, a discernible trend emerges wherein the SC fault model exerts a more pronounced influence on the rover's DC motor model. The introduction of Model B fault implementation disrupts the rover's path tracking, whereas the incorporation of Model A results in the rover faithfully adhering to the prescribed path.

Table II shows the magnitude of the residuals generated by KF when the SC fault models (A and B) are introduced to the DC motor model with several fault ratios δ. An analysis of the generated residual, as obtained through the utilization of the model-based KF fault detection method, reveals that upon introducing Model B to the system, the residual exhibits a higher magnitude compared to its counterpart with Model A integration. This discrepancy imparts

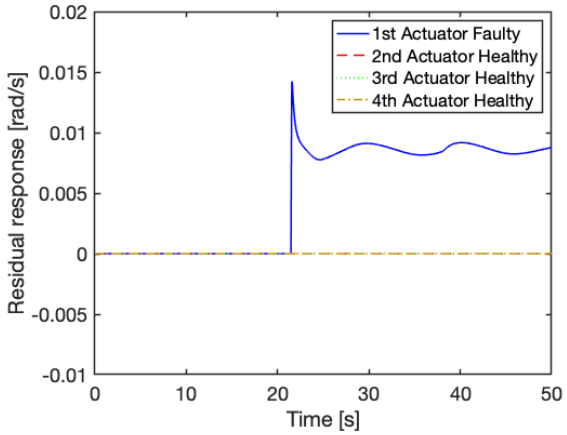

Fig. 13. Residuals of four wheels velocities with 30% SC fault (Model B) ratio

TABLE II
SC FAULT MODELS IMPLEMENTING RESIDUALS DATA

δ	SC Model	r(rad/s)
10%	Model A	0.00003
	Model B	0.0016
20%	Model A	0.00006
	Model B	0.004
30%	Model A	0.00009
	Model B	0.008
40%	Model A	0.00012
	Model B	0.013
50%	Model A	0.00015
	Model B	0.02
60%	Model A	0.00019
	Model B	0.04
70%	Model A	0.00022
	Model B	0.08
80%	Model A	0.00025
	Model B	0.17
90%	Model A	0.00029
	Model B	0.38

greater flexibility in the selection of a fixed threshold for fault detection. Based on the desired limit of the SC fault ratio a fixed threshold can be selected to detect and isolate the fault. A fixed threshold could be chosen to detect the fault for model A, but the small residual response is a drawback. If the uncertain dynamics of the DC motor are added to the model, the small threshold could incorrectly expose a SC fault. Therefore, Model B of the SC fault has a better chance of being detected and isolated than Model A.

VI. Conclusion

Increasing the reliability and trustworthiness of PERs is an essential issue for the space exploration milieu. Because the actuators (DC motors) of a PER are vulnerable to faults, like a SC fault, that conduct system failure, the ability to diagnose faults is crucial. Establishing a fault model supersedes the physical system experimentation to study the fault detection algorithms.

In this work, two models of SC fault (Model A and Model B) are implemented to study and analyse the effect on the rover's model performance and health monitoring. The impact of the SC fault Model A on the DC motor responses (current and angular velocity) is small compared to the effect of Model B. The results show that the rover model performance is affected by fault Model B in the rover's path following process. Also, the analysis approved that the KF-based fault detection algorithm was able to detect the SC fault of Model B better than Model A. It is clear that Model B provides a SC fault representation that has an impact on the rover's model and is easily detectable by using the KF-based fault detection method.

References

[1] Ellery A. Planetary rovers: robotic exploration of the solar system. Springer; 2015.

[2] Isermann R. Fault-diagnosis systems: an introduction from fault detection to fault tolerance. Springer Science & Business Media; 2005.

[3] Al Oufi S, Shilliday SR, Woods J, McGookin EW. Implementation of FMEA in the Development of Actuator and Sensor Fault Models for a Rover Health Monitoring Simulation. In: 2022 UKACC 13th International Conference on Control (CONTROL). IEEE; 2022. p. 116-21.

[4] Isermann R. Mechatronic systems: fundamentals. Springer Science & Business Media; 2007.

[5] Blanke M, Kinnaert M, Lunze J, Staroswiecki M, Schröder J. Diagnosis and fault-tolerant control. vol. 2. Springer; 2006.

[6] Ullah Z, Hur J. A comprehensive review of winding short circuit fault and irreversible demagnetization fault detection in PM type machines. Energies. 2018;11(12):3309.

[7] Zhang J, Zhan W, Ehsani M. On-line diagnosis of inter-turn short circuit fault for DC brushed motor. ISA transactions. 2018;77:179-87.

[8] Aubert B, Regnier J, Caux S, Alejo D. Kalman-filter-based indicator for online interturn short circuits detection in permanent-magnet synchronous generators. IEEE Transactions on Industrial Electronics. 2014;62(3):1921-30.

[9] Shilliday SR, Swinton S, Al Oufi S, McGookin EW, Thomson DG, Worrall KJ. Friction Modelling With Slip For Planetary Exploration Rovers. 2023.

[10] Fossen TI. Guidance and control of ocean vehicles; 1994.

[11] Worrall KJ. Guidance and search algorithms for mobile robots: application and analysis within the context of urban search and rescue. University of Glasgow; 2008.

[12] Farooq JA, Raminosoa T, Djerdir A, Miraoui A. Modelling and simulation of stator winding inter-turn faults in permanent magnet synchronous motors. COMPEL-The international journal for computation and mathematics in electrical and electronic engineering. 2008;27(4):887-96.

[13] Grewal MS, Andrews AP. Kalman filtering: Theory and Practice with MATLAB. John Wiley & Sons; 2014.